Dalton Transactions

PAPER

Synthesis, photovoltaic performances and TD-DFT modeling of push–pull diacetylide platinum complexes in TiO_2 based dye-sensitized solar cells†

Cite this: *Dalton Trans.*, 2014, **43**, 11233

Sébastien Gauthier,*[a] Bertrand Caro,[a] Françoise Robin-Le Guen,[a] Nattamai Bhuvanesh,[b] John A. Gladysz,[b] Laurianne Wojcik,[c] Nicolas Le Poul,[c] Aurélien Planchat,[d] Yann Pellegrin,[d] Errol Blart,[d] Denis Jacquemin*[d,e] and Fabrice Odobel*[d]

Received 28th January 2014,
Accepted 17th April 2014

DOI: 10.1039/c4dt00301b

www.rsc.org/dalton

In this joint experimental–theoretical work, we present the synthesis and optical and electrochemical characterization of five new bis-acetylide platinum complex dyes end capped with diphenylpyranylidene moieties, as well as their performances in dye-sensitized solar cells (DSCs). Theoretical calculations relying on Time-Dependent Density Functional Theory (TD-DFT) and a range-separated hybrid show a very good match with experimental data and allow us to quantify the charge-transfer character of each compound. The photoconversion efficiency obtained reaches 4.7% for **8e** (see TOC Graphic) with the tri-thiophene segment, which is among the highest efficiencies reported for platinum complexes in DSCs.

Introduction

Dye sensitized solar cells (DSCs) are attractive photovoltaic devices for low cost electricity production.[1] Transition metal coordination complexes, especially polypyridine ruthenium complexes, have proven to be particularly efficient sensitizers for this technology.[2] Compared to ruthenium complexes, platinum complexes remain rather unexplored as sensitizers for DSCs,[3] despite their valuable photoredox properties.[4] In fact, platinum acetylide complexes have found widespread applications as structural building blocks in the areas of supramolecular self-assembly[5] and functional materials science.[3h,i,6] Moreover, due to the linear geometry of the alkynyl unit and its conjugated character, these platinum acetylide complexes have displayed interesting properties such as non-linear optical (NLO) responses, luminescence, and electrical conductivity.[5a,e,7] Recently, platinum acetylide complexes have been used as dyes in photoinduced energy and electron transfer arrays and for hydrogen production.[4a,8] In two previous reports, Tian and co-workers developed a series of platinum acetylide complexes showing promising photoconversion efficiencies.[3h,i]

We have combined the proaromatic pyranylidene ligand[9] with bis-acetylide platinum units and systematically varied the nature and the length of the spacer connected to the cyano acrylic anchoring group (Chart 1). The pyranylidene which acquires a pyrylium aromatic character on charge transfer has been successfully used in the push–pull NLO-chromophore[10] and in organic dyes for solar cells.[11] The D-π-M-π-A combination resulted in dyes exhibiting an effective broadening of the light absorption spectrum and, consequently, in a higher photocurrent production and a higher photoconversion efficiency (PCE).

In the field of DSCs, like in many others, joint theoretical–experimental analyses are particularly useful considering the complexity of the processes involved in these devices. Indeed, the electron injection into the semiconductor comes after the

[a]*Institut des Sciences Chimiques de Rennes, UMR CNRS 6226, IUT de Lannion, rue Edouard Branly, BP 30219, F22302 Lannion Cedex, France. E-mail: sebastien.gauthier@univ-rennes1.fr; Fax: +33 296469354; Tel: +33 296469344*

[b]*Department of Chemistry, Texas A&M University, PO Box 30012, College Station, Texas 77842-3012, USA*

[c]*Laboratoire de Chimie, Electrochimie Moléculaires et Chimie Analytique UMR CNRS 6521, Université de Bretagne Occidentale, 6 Avenue Le Gorgeu, 29238 Brest Cedex 03, France*

[d]*Université LUNAM, Université de Nantes, CNRS, Chimie et Interdisciplinarité: Synthèse, Analyse, Modélisation (CEISAM), UMR 6230, 2 rue de la Houssinière, 44322 Nantes Cedex 3, France. E-mail: Fabrice.Odobel@univ-nantes.fr; Fax: +33 251125402; Tel: +33 251125429*

[e]*Institut Universitaire de France, 103, bd Saint-Michel, F-75005 Paris Cedex 05, France. E-mail: Denis.Jacquemin@univ-nantes.fr*

†Electronic supplementary information (ESI) available: Synthetic and characterization data of new compounds, general crystallographic data of complex **5**, voltammetry cyclic and density difference plots for **8b** and **8e**. Crystallographic data have been deposited in the Cambridge database. CCDC 982741. For ESI and crystallographic data in CIF or other electronic format see DOI: 10.1039/c4dt00301b

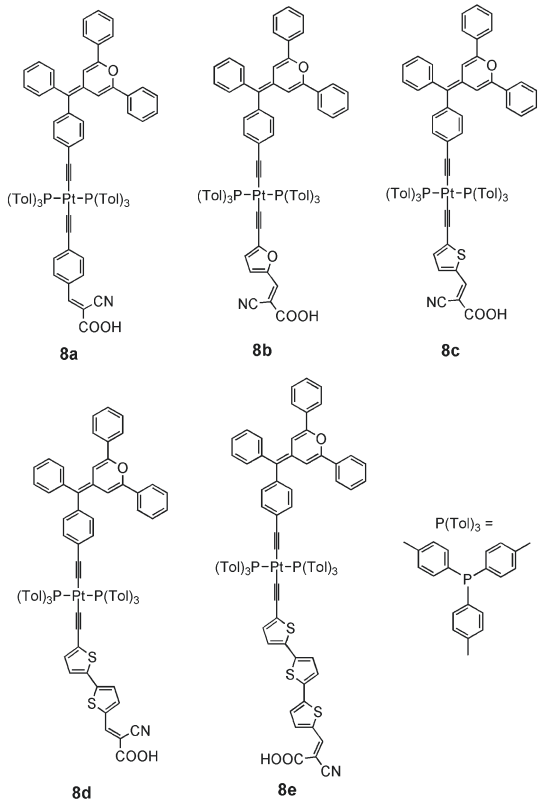

Chart 1 Chemical structures of platinum complexes **8a–e** investigated in this work.

electronic excitation of the dye: the light-to-electricity conversion is therefore triggered by the formation of an electronically excited state. In particular, charge-transfer (CT) excited states where the absorption of a photon induces a strong intramolecular separation between the electron and the hole are particularly beneficial to DSC's efficiency. Therefore, the optimisation of the CT properties of the dyes is of particular interest. However, excited states are extremely short-lived, making their complete experimental characterization particularly difficult and often costly. For this reason, the use of theoretical tools to investigate these electronically excited states is becoming increasingly popular. In particular, Time-Dependent Density Functional Theory (TD-DFT), which provides an accurate result while maintaining reasonable computational time, has emerged as the most applied theory in the field. Indeed, numerous recent publications on DSCs have reported results combining theoretical and experimental data.[12] As an example of the growing interest in TD-DFT simulations, theoretical approaches have been developed to quantify the CT nature of the excited states of dipolar dyes.[13] One of these theoretical approaches is also used in this work to provide a CT distance (expressed in Å), subsequently paving the way for an *in-silico* optimisation of the CT properties.

Here we present a synthesis route of five new di-acetylide platinum-based complexes **8a–e** comprising a pyranylidene ligand and functional groups (*i.e.* phenyl, furan, bi- and trithiophene) of different nature and lengths as linkers separating the Pt unit from the anchoring cyanoacetic group. These complexes were prepared, fully characterized and evaluated in TiO_2-based DSCs.

Experimental

Chemicals and materials

All reactions were conducted under a dry argon atmosphere using Schlenk techniques, but workups were carried out in air. THF was dried using a solvent dispensing system (Seca Solvent System). Hexanes, CH_2Cl_2, $CHCl_3$, ethyl acetate (3 × ACS grade), K_2CO_3 (99% Alfa Aesar), silica gel (Acros or Fluoroflash), alumina (Al_2O_3, neutral, Brockmann I, for chromatography, 50–200 μm, Acros), copper(I) iodide (99.999%, Aldrich), diethylamine (99.5%, Aldrich), piperidine (99% Alfa Aesar) and cyanoacetic acid (99%, Alfa Aesar) were used as received. The complexes *cis*-$[Pt(P(Tol)_3)_2Cl_2]$ and tributyl(2,6-diphenyl-4*H*-pyran-4-yl)phosphonium tetrafluoroborate (**1**) were prepared as previously described.[14,15] The aldehydes **6a–e** were prepared from commercially available aryl bromide precursors: 4-bromobenzaldehyde, 5-bromo-2-furaldehyde, 5-bromothiophene-2-carboxaldehyde, 5-bromo-2,2′-bithiophene-5′-carboxaldehyde and 5″-bromo-2,2:5′,2″-terthiophene-5-carboxaldehyde (5 × Aldrich).[16] A CH_2Cl_2 solution of **5** was layered with pentanes and kept at room temperature under an inert atmosphere. After 3 days, colorless column crystals of suitable size for single crystal X-ray diffraction measurements were obtained.

Physical characterization

Elemental analysis was performed at the *Centre Régional de Mesures Physiques de l'Ouest* (CRMPO, University of Rennes 1) using a Microanalyseur Flash EA1112 CHNS/O Thermo Electron. MALDI spectra were recorded on an Applied Biosystems Voyager-DE STR spectrometer with DCTB as the matrix at the Laboratory for Biological Mass Spectrometry, Texas A&M University, USA. NMR spectra were recorded on a Varian NMRS 500 MHz spectrometer or a Bruker Advance NMRS 300 MHz spectrometer and referenced as follows: ^{1}H NMR, residual $CHCl_3$ (δ, 7.24 ppm); $^{13}C\{^1H\}$ NMR, internal $CDCl_3$ (δ, 77.0 ppm); $^{31}P\{^1H\}$ external H_3PO_4 (δ, 0.00 ppm). IR spectra were recorded on a Shimadzu IRAffinity-1 spectrometer with a Pike MIRacle ATR system (diamond crystal). UV-visible spectra were recorded on a Shimadzu UV-1800 spectrometer. Emission spectra were recorded using a PTI QuantaMasterTM 40 fluorescence spectrofluorometer. Thin-layer chromatography (TLC) was carried out on EMD Silica Gel 60 F254 or EMD aluminum oxide 60 F254 (neutral) plates that were visualized with 254 nm or 365 nm UV light.

X-ray crystallographic data collection and refinement

Single crystal X-ray diffraction data were collected using a Bruker GADDS (Cu-Kα) diffractometer.[17] Cell-now[18] was used to determine unit cell from 180 data frames. After a careful examination, an extended data collection procedure (26 sets)

was initiated using omega and phi scans. Integrated intensity information for each reflection was obtained by reduction of the data frames with APEX2.[19] SADABS was employed to correct the data for absorption effects.[20] The structure was solved by direct methods (SHELXS) and refined (SHELXL-97, weighted least squares refinement on F^2) using APEX2[19] and OLEX2, respectively.[20,21] Non-hydrogen atoms were refined with anisotropic thermal parameters. The parameters were refined by weighted least squares refinement on F^2 to convergence.[20] The absence of additional symmetry was verified using PLATON,[22] which also indicated a void of about 33 Å[19] with a residual electron density (1.03 e^- $Å^{-3}$) suggesting the presence of partially occupied solvent, which was assumed to be water (10% occupancy). The crystallographic data and the result of refinements of **5** (see below for structure) are summarized in ESI.†

Cyclic voltammetry

The electrochemical studies were performed in a glovebox (Jacomex) (O_2 < 1 ppm, H_2O < 1 ppm) with a home-made 3-electrode cell (WE: Pt, RE: Ag wire, CE: Pt). Ferrocene standard was added at the end of each experiment. The redox potential of the Fc^+/Fc couple in CH_2Cl_2/NBu_4PF_6 was measured experimentally with reference to the standard calomel electrode (SCE): $E^0(Fc^+/Fc)$ = 0.47 V *vs.* SCE, and recalibrated *vs.* NHE assuming that E^0(SCE) = 0.24 V *vs.* NHE. The potential of the cell was controlled by an AUTOLAB PGSTAT 100 (Metrohm) potentiostat monitored by the NOVA© software (Metrohm). Dichloromethane was freshly distilled from CaH_2 and kept under Ar in the glovebox. The supporting salt NBu_4PF_6 was synthesized from NBu_4OH (Fluka) and HPF_6 (Aldrich). It was then purified, dried under vacuum for 48 hours at 100 °C, and then kept under N_2 in the glovebox.

Theoretical

All quantum mechanical simulations have been performed with the latest version of the Gaussian09 program.[23] The optical spectra of the structures represented in Chart 1 have been analyzed. However, since the tolyl groups bonded to the phosphorus atoms do not play an important role in the optical features of individual dyes, methyl groups were used in the calculation in order to reduce the computational burden. We followed a methodology similar to the one successfully used previously for similar DSC dyes.[13] Therefore, we selected the PBE0 global hybrid exchange-correlation functional[24] for determining structural parameters and the CAM-B3LYP[25] range-separated hybrid functional to compute the optical properties (TD-DFT part). This choice was motivated by the charge-transfer nature of several excited-states. First, geometry optimizations and frequency calculations in dichloromethane were performed using the Polarizable Continuum Model (PCM) solvent model,[26] and the LanL2DZ basis with additional polarization functions.[27] This allowed the nature of the structures (true minima) to be ascertained and the infrared spectra to be obtained. The theoretical (harmonic) vibrational frequencies reported below were scaled by a factor of 0.96 to account for anharmonicity effects. In the second step, the first forty singlet lowest-lying excited-states were determined within the vertical PCM-TD-DFT approximation using the same basis set, but augmented with diffuse orbitals.[28] The latter calculations were performed with the standard non-equilibrium LR-PCM (Linear-Response PCM) approach.[26] For the first strongly dipole allowed states, we determined the difference in electronic density between ground and excited-states with TD-DFT, which allows for chemically sound representations of the impact of the electronic transitions. A threshold of 0.0004 u.a. was used to plot these differences. A recently developed approach for quantifying the charge transfer[13] has been applied in order to further characterize the dyes (see the Introduction).

Results and discussion

Synthesis of the sensitizers

The synthesis of the complexes requires the starting material, 4-[(4-ethynyl-phenyl)-phenyl-methylene]-2,6-diphenyl-4*H*-pyran **4**, whose preparation was accomplished in two steps as shown in Scheme 1. The diphenylpyranylidene unit **3** was produced by a Wittig reaction of tributyl(2,6-diphenyl-4*H*-pyran-4-yl)-phosphonium tetrafluoroborate **1**[15] with 4-(2-trimethylsilyl-ethynyl)benzophenone **2**[29] in the presence of *n*-BuLi in good yield.[30] The trimethylsilyl compound **3** was converted to the corresponding terminal alkyne **4** quantitatively by desilylation under basic conditions.[31]

The synthetic approach to platinum complexes **8a–e**, shown in Scheme 2, was based upon the well documented substitution of platinum chloride complexes by terminal acetylenes.[3i,32] The precursor complex **5** was prepared by reaction of **4** with *cis*-$[Pt(P(Tol)_3)_2Cl_2]$ in the presence of a catalytic amount of copper(I) iodide and diethylamine at 60 °C. In this reaction, an excess of *cis*-$[Pt(P(Tol)_3)_2Cl_2]$[14] was necessary to minimize the formation of the undesirable oligomeric byproducts. Subsequent coupling with the corresponding aldehydes **6a–e**[16] under a conventional cross-coupling condition resulted in compounds **7a–e**. The final products **8a–e** were then obtained in good yields (80–95%) by Knoevenagel reactions of the corresponding precursors with cyanoacetic acid in the presence of piperidine.

The new compounds were characterized by IR, NMR (^1H, ^{31}P, and ^{13}C), high-resolution mass spectrometry and satis-

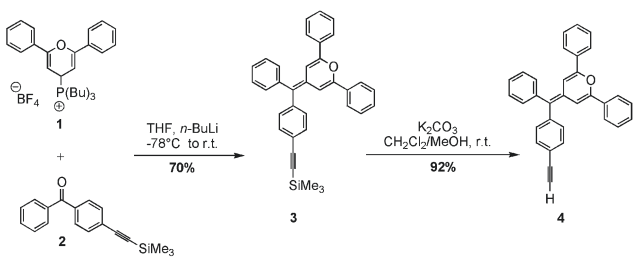

Scheme 1 Preparation of compound **4**.

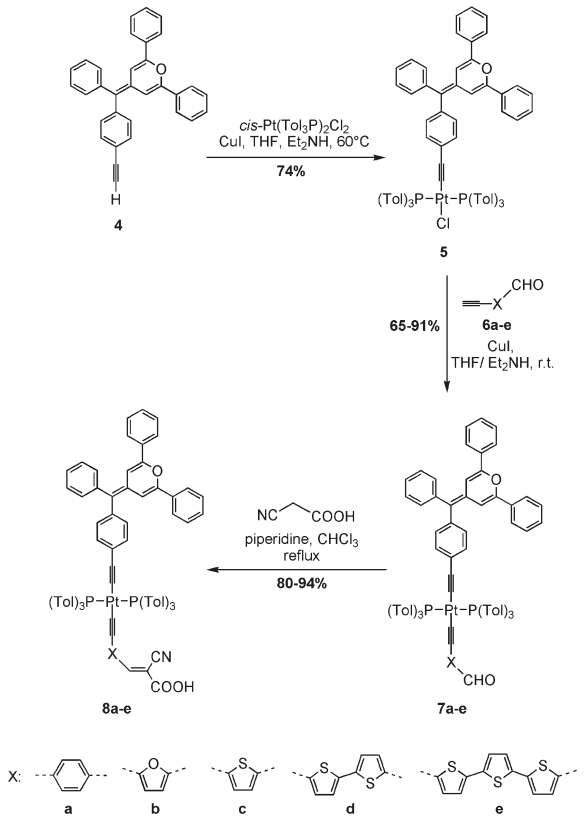

Scheme 2 Synthesis route to the dyes **8a–e**.

factory microanalyses (see the ESI†). These data fully supported the proposed structures. Single crystals of complex **5** were grown by slow diffusion of pentane into a concentrated solution of **5** in dichloromethane under an inert atmosphere. The X-ray structure was determined, and the resulting thermal ellipsoid plot is given in Fig. 1. Complex **5** was crystallized in the $P\bar{1}$ space group. The platinum atom is four-coordinated in a slightly distorted square planar geometry. As expected, the molecular structure shows that the platinum center is attached to a chloride, a pyranylidene ligand and that two tri(*p*-tolyl)-

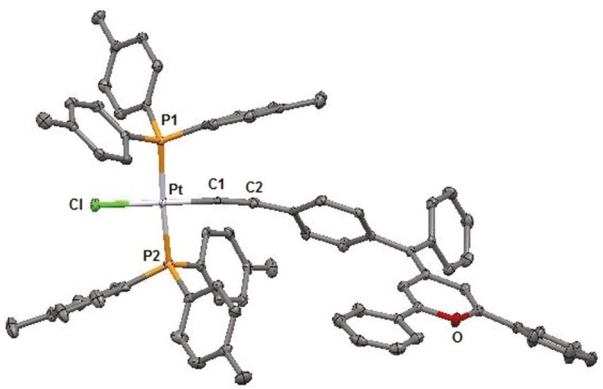

Fig. 1 Perspective view of **5** with thermal ellipsoids drawn at the 50% probability level; solvent molecules and hydrogen atoms are omitted for clarity.

phosphines are coordinated to the platinum center in a *trans* arrangement. The bond lengths and angles about platinum are unexceptional.[33] The C2≡C1–Pt–Cl chain is almost linear, with angles at C2≡C1–Pt and C1–Pt–Cl of 174.2(3)° and 178.33(9)°, respectively. The Pt–C1 distance of 1.952(3) Å and the C1≡C2 bond length of 1.209(4) Å lie in the range observed for other platinum coordinated acetylide ligands.[34]

The IR spectra of the alkynyl complexes **8a–e** contain a $\nu_{C\equiv C}$ band at *ca.* 2112 cm^{-1} assigned to the metal-bonded alkynyl group. The $\nu_{C\equiv N}$ (around 2160 cm^{-1}), $\nu_{C=O}$ (around 1694 cm^{-1}) and $\nu_{C=C}$ (around 1575 cm^{-1}) bands are characteristic of the cyanoacrylic acid function. The ^{1}H NMR spectrum of the ligand **4** shows characteristic signals such as the vinylic H resonance of the methylenepyran core which appears as two doublets (δ = 6.72 and 6.69 ppm; $^4J_{H,H}$ = 2.0 Hz), a multiplet signal for the disubstituted phenyl ring (δ = 7.67–7.37 ppm) and a singlet for the alkyne proton (δ = 3.14 ppm). In the complex **5**, due to the inductive effect of the platinum coordination, the hydrogens of the disubstituted phenyl (δ = 6.77 and 6.04 ppm) and the vinylic protons (δ = 6.61 and 6.60 ppm) are upfield shifted. A similar shift effect has been observed for the series **7a–e** and **8a–e**. This series of complexes display essentially identical ^{1}H NMR signals for the tri(*p*-tolyl)phosphines, the pyranylidene ligand, the π-conjugated spacer and the aromatic protons. The ^{1}H and ^{13}C NMR spectra of the complexes **7a–e** show expected signals such as a singlet at *ca.* δ = 9.80 ppm assigned to the aldehyde proton and a peak of the aldehyde carbon at *ca.* δ = 180 ppm. The ^{1}H NMR spectra of the cyanoacetic acid complexes **8a–e** exhibit a characteristic singlet at *ca.* δ = 8.10 ppm assigned to the proton attached to the β-carbon atom of the cyanoacetic acid group. Finally, the ^{31}P NMR spectra of all complexes **8a–e** exhibit a sharp singlet, diagnostic of *trans* geometries of the phosphine ligands around the platinum (for example δ = 17.4 ppm, $^1J_{Pt-P}$ = 2600 Hz, for **8a**). The approximately 3 ppm shift of this singlet upon going from **5** to **8a** can be attributed to the electron π-conjugated bridges.

Electronic absorption and emission spectra

The UV-Vis absorption and emission spectra of dyes **8a–e** recorded in a dilute dichloromethane solution are shown in Fig. 2 whereas the spectroscopic data are collected in Table 1.

The dye **8a** exhibits only one major band at 415 nm, but in contrast **8b–d** dyes display two major prominent bands on their UV-visible spectra, $\lambda^{abs}_{max}(2)$ in the 300–400 nm range and $\lambda^{abs}_{max}(1)$ in the 400–600 nm range. As shown below, the higher-energy absorption bands [$\lambda^{abs}_{max}(2)$] correlate with intra-ligand charge transfer (ILCT) transitions (π–π*) centered on the pyran part, whereas the lower-energy absorption band [$\lambda^{abs}_{max}(1)$] corresponds to ILCT transitions (π–π*) more localized on the cyanoacetic part (see TD-DFT calculations below for more details). The latter band corresponds to the light harvesting of the complexes in the visible region. The red-shift of the maximum absorption of **8d** and **8e**, as compared with that of **8c**, can be explained by the enhanced electron delocalization over the oligothiophene spacer of increasing length. Moreover,

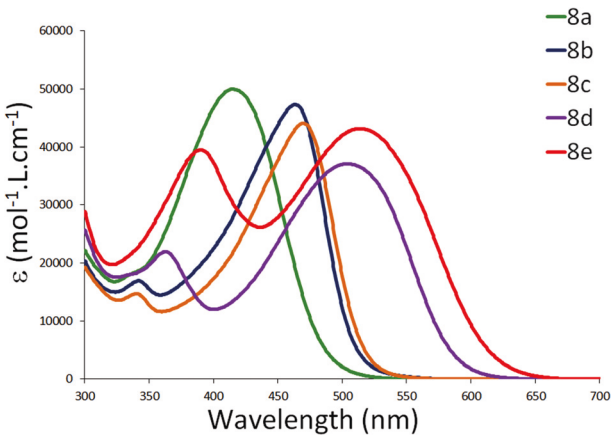

Fig. 2 UV-Vis absorption spectra of dyes **8a–e** in dichloromethane solution (3×10^{-5} M) at room temperature.

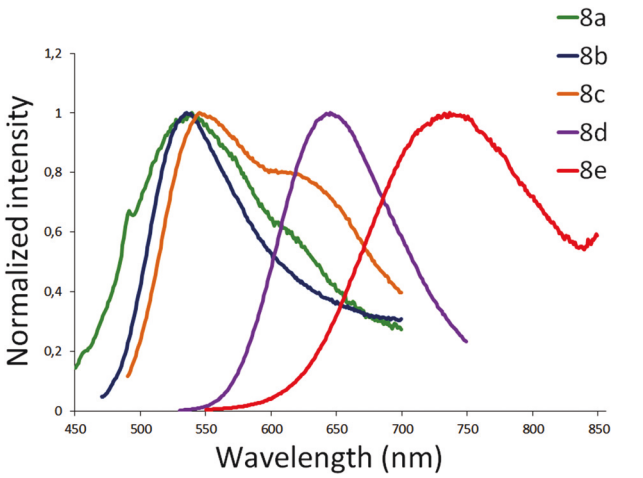

Fig. 3 Emission spectra recorded in CH_2Cl_2 solution (5×10^{-6} M) at room temperature for dyes **8a–e**.

Table 1 Absorption and fluorescence properties of the dyes **8a–e** recorded in dichloromethane at room temperature

Dye	$\lambda_{max}^{abs}(2)$/nm ($\varepsilon \times 10^4$ M^{-1} cm^{-1})	$\lambda_{max}^{abs}(1)$/nm ($\varepsilon \times 10^4$ M^{-1} cm^{-1})	λ_{max}^{emi}/nm
8a	—	415 (5.0)	539
8b	342 (1.7)	463 (4.7)	535
8c	342 (1.5)	469 (4.4)	545
8d	363 (2.2)	504 (3.7)	645
8e	390 (3.9)	514 (4.3)	736

Table 2 Voltammetry data for compounds **4**, **5**, **8a–e** and **9** (1 mM) in CH_2Cl_2/NBu_4PF_6 0.1 M (*E*/V *vs.* Fc^+/Fc[a], v = 0.1 V s^{-1}); platinum working electrode

Dye	$E_{pa}(1)$	$E^0(1)$	$E_{pa}(2)$	$E^0(2)$	$E_{pc}(3)$	$E_{pc}(4)$
8a	0.18	0.14	0.41	0.38	−1.37	−0.85
8b	0.18	0.14	0.43	0.39	−1.39	−0.86
8c	0.17	0.13	0.42	0.37	−1.25	−0.86
8d	0.19	0.14	0.42	0.38	−1.35	−0.84
8e	0.18	0.14	0.45	0.41	−1.43	−0.85
4	0.30	0.26	0.62			−0.83
9	0.30					−0.78
5	0.18	0.14	0.41	0.37		−0.85

[a] $E^0(Fc^+/Fc)$ = 0.47 V *vs.* SCE in CH_2Cl_2/NBu_4PF_6 (measured experimentally) and $E^0(SCE)$ = 0.24 V *vs.* NHE.

the phenyl spacer in complex **8a** spans a shorter π-conjugation length than the furan or the thiophene linker as evidenced by the blue shift of the ILCT band. In addition, these dye molecules exhibit molar absorption coefficients about three times greater than that of the well-known **N719** ruthenium sensitizer (**N719**: *cis*-bis(isothiocyanato)bis(2,2′-bipyridyl-4,4′ dicarboxylato) ruthenium(II), di-tetrabutylammonium) which displays a molar absorption coefficient of 1.47×10^4 M^{-1} cm^{-1} at 535 nm,[35] while **8d** and **8e** absorption coefficients are 3.7×10^4 M^{-1} cm^{-1} at 504 nm and 4.37×10^4 M^{-1} cm^{-1} at 514 nm, respectively.

All the complexes **8a–e** are emissive at room temperature (Fig. 3), a feature that allows the determination of the zero–zero excited state energy (E_{00}) with the wavelength at the intersection of the electronic absorption and emission spectra (see below). We note that two dyes, **8a** and **8c**, seem to present a second emission band at longer wavelengths, and this is clearly unexpected. Nevertheless, as we use only the emission spectra to determine the zero–zero energies, this outcome is not relevant for our purposes and was not further investigated.

Electrochemical measurements

The redox behavior of each of the platinum complexes **8a–e** (Chart 1) was examined by cyclic voltammetry (CV) in CH_2Cl_2/NBu_4PF_6 0.1 M on a platinum working electrode (see Table 2 for the electrochemical data). In oxidation, two reversible systems at *ca.* $E^0(1)$ = 0.14 V and $E^0(2)$ = 0.38 V *vs.* Fc^+/Fc were systematically detected (see Table 2).[36] In addition, all complexes displayed an irreversible reduction peak at *ca.* $E_{pc}(3)$ = −1.4 V (Fig. 4 and Table 2). When scanning up to 1.0 V, an additional peak at 0.80 V (see Fig. S1B, in the ESI,† curve b, peak *), and two reduction peaks on the second cycle at $E_{pc}(6)$ = −0.65 and $E_{pc}(4)$ = −0.80 V (Fig. 4 and Table 2) were detected. The former reduction peak was not observed for all complexes whereas the latter systematically appeared. In order to identify the redox processes, the analogous compound 4-[(4-ethynyl-benzylidene)-2,6-diphenyl-4*H*-pyran **9** was investigated by CV.[37] It underwent irreversible oxidation at $E_{pa}(1)$ = 0.30 V and displayed irreversible reduction at $E_{pc}(4)$ = −0.78 V on the backscan (Fig. S1A,† curve b, and Table 2). This reduction peak can be assigned to the reduction of the bis-pyrylium species, resulting from a C–C coupling reaction after monoelectronic oxidation of the pyran, as previously reported.[38] Compound **4**, which contains an additional phenyl ring on the ethynylene bridge, behaved differently than **9**. For this compound, the first oxidation process was no longer irreversible at the timescale of the experiment (i_{pa}/i_{pc} = 0.6 at 0.1 V s^{-1}) and a second oxidation process was detected at $E_{pa}(2)$. For the Pt-complex **5**, cyclic voltammetry showed two reversible systems at $E^0(1)$ = 0.14 V and $E^0(2)$ = 0.41 V (Table 2) and one irrevers-

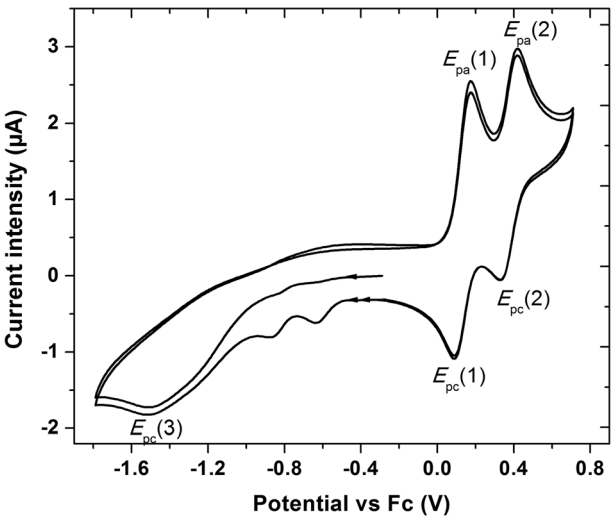

Fig. 4 Cyclic voltammograms of **8c** (1 mM) (v = 0.1 V s^{-1}, 2 cycles, E/V *vs.* Fc^+/Fc) at a Pt working electrode in CH_2Cl_2/NBu_4PF_6 (0.1 M).

ible cathodic peak at $E_{pc}(4)$ = −0.85 V. Unlike complexes **8a–e**, neither an oxidation peak at 0.8 V nor a reduction peak at $E_{pc}(3)$ was detected for this complex (Fig. S1B,† curve a). Exhaustive electrolysis was performed on compounds **4** and **5** at a constant potential value between the two oxidation processes (1) and (2). For these experiments, coulometric measurements indicated that the first oxidation wave corresponded to a one-electron process. Interestingly, Rotating-Disk Electrode Voltammetry (RDEV) showed the presence of pyrylium cations in solution for the complex **5** after full electrolysis (Fig. S1C†), while those cations were not detected in compounds **4** (inset of Fig. S1C†) and **9**. From these results, we can conclude the following:

(i) Both reversible processes at $E^0(1)$ and $E^0(2)$ can be ascribed to the successive monoelectronic oxidations of the pyrylidene moiety. They are only slightly affected by the variation of the linker (phenyl, furanyl, thiophenyl, *etc.*) within the electron-withdrawing part of the platinum complexes. The potential difference value $\Delta E^0(1\text{–}2) = E^0(2) - E^0(1)$ is low (240–250 mV), indicating that the oxidation of the pyrylium radical cation requires a relatively small quantity of energy.

(ii) $E_{pa}(1)$ and $E_{pa}(2)$ values are significantly lower for complexes **8a–e** and **5** than for compound **4**, suggesting a stabilization of the radical pyrylium cation and dicationic species in the presence of platinum.

(iii) The phenyl moiety present in the ethylene bridge of the pyran for compounds **8a–e**, **4** and **5** has a strong influence on the C–C coupling reaction. This might be due to both steric (hindrance of the phenyl and metallic moiety) and electronic effects, since the stabilization of the radical cation through delocalization of the charge may deactivate the C–C coupling.

(iv) The $E_{pc}(3)$ irreversible peak can be ascribed to the reduction of the Pt-cyano-acrylic moiety of the complexes **8a–e**. However, the broad shape of the peaks does not enable us to rationalize the exact influence of the linker on the reduction electron transfer process.

In conclusion, the voltammetry studies provided not only information about the redox properties of the complexes **8a–e** to be obtained, but also the determination of injection (ΔG_{inj}) and regeneration (ΔG_{reg}) Gibbs free energies (Table 3). Complexes **8a–e** can be mono-electronically oxidized at $E_{pa}(1)$ in this electrolyte. The resulting pyrylium species are relatively stable as shown by exhaustive electrolysis. This property is valuable for DSC applications since electrochemical stability of the oxidized species is a key feature for achieving a long lifespan of the cell. For all complexes, very negative values of ΔG_{inj} were calculated, implying that the injection yields for **8a–e** were likely to be very similar and close to unity (Table 3). Likewise, the regeneration step is endowed with an identical Gibbs free energy, regardless of the complex. All these thermodynamic considerations indicate that complexes **8a–e** could potentially be efficient sensitizers in TiO_2 based DSCs.

TD-DFT calculations

First principle calculations were performed to further characterize the nature of the excited-states in **8a–e**. A preliminary step to optical simulations is to ascertain the quality of the structures. The connecting unit and the donor group of **8a–e** and **5** being the same, we have first used **5** for this assessment. For compound **5**, the computed Pt–C1 (C1≡C2) distance is 1.926 (1.236) Å, which deviates from experiments by 0.026 (0.023) Å. This lies in the typical error range of DFT calculations. Secondly, we compared the theoretical IR frequencies to the experimental IR data. In compound **8a**, DFT gives an intense band at 2090 cm^{-1} for the stretching of the carbon–carbon triple bonds which corresponds to the band at 2112 cm^{-1} observed experimentally. Likewise, the theoretical $\nu_{C\equiv N}$ band calculated by DFT at 2231 cm^{-1} reasonably matches the experimental value found at 2160 cm^{-1} (see above). Lastly, the $\nu_{C=O}$ and $\nu_{C=C}$ stretching, measured at *ca.* 1694 cm^{-1} and 1575 cm^{-1}, were computed at 1739 cm^{-1} and 1560 cm^{-1}, respectively. The theoretical simulation of the electronic absorption spectra is displayed in Fig. 5. The computed and the experimental absorption spectra (Fig. 2) are in very good agreement with each other, and this holds for both the positions and the relative intensities of all absorption peaks,

Table 3 ΔG_{inj} and ΔG_{reg} values for the complexes **8a–e**

Dye	E_{ox} (V *vs.* Fc^+/Fc)	E_{00} (eV)	ΔG_{inj} (eV)	$\Delta G_{reg}{}^a$ (eV)	$\Delta G_{reg}{}^b$ (eV)
8a	0.14	2.66	−1.37	−0.49	−0.04
8b	0.13	2.51	−1.23	−0.48	−0.03
8c	0.14	2.47	−1.18	−0.49	−0.04
8d	0.14	2.14	−0.99	−0.49	−0.04
8e	0.14	2.02	−0.87	−0.49	−0.04

[a] E_{CB,TiO_2} = −1.15 V *vs.* Fc^+/Fc; $E^0(I_3^-/I^-)$ = −0.35 V *vs.* Fc^+/Fc. [b] $E^0(I_2^{\bullet-}/I^-)$ = 0.1 V *vs.* Fc^+/Fc. E_{00} calculated from the wavelength (λ_{inter}) at the intersection of normalized emission and absorption spectra, with the equation E_{00} (eV) = 1240/λ_{inter}.

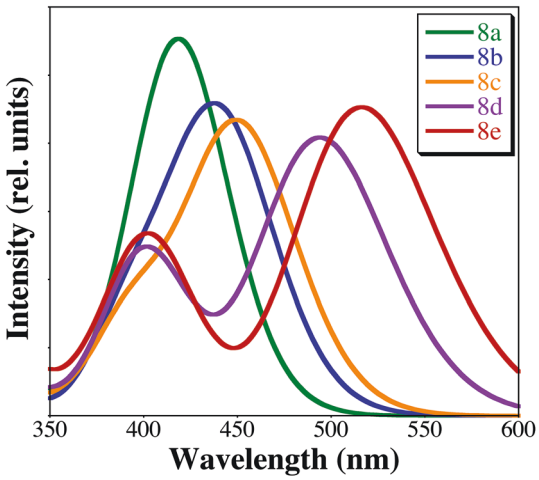

Fig. 5 Computed absorption spectra obtained from convolution with a 0.40 eV Gaussian of the TD-DFT (vertical) stick spectrum.

except for the intensity of the second absorption band of **8e**, which is slightly underestimated by the calculations. The computed maximum absorption wavelengths are gathered in Table 4. The order of these wavelengths **8a** < **8b** < **8c** < **8d** < **8e** is in full agreement with the experimental data (Table 1), whereas the mean absolute deviation of the $\lambda_{max}^{abs}(1)$ is as small as 12 nm, a trifling deviation for TD-DFT calculations on large dyes, thus confirming the accuracy of the selected protocol.[39]

The density difference plots representing the electronic changes between the ground and excited states are shown in Fig. 6. As expected, the cyanoacetic moiety acts as an electron acceptor (mostly in red), which is favorable for charge injection as it pulls the electronic density close to the TiO_2 surface. Interestingly, the excited state is highly delocalized. The pyran donor only plays a major role in the first transition of **8a** and in the second transition of **8e**. For the first transition in the other dyes, the changes are mainly localized to the thiophene rings and anchoring groups. It is also noteworthy that all CT distances are *ca.* 5 Å (Table 4). While this indicates that the CT strength is not relevant to discriminate among the dyes in the present case, a 5 Å CT should be considered as particularly large within the selected model.[13a–c] In other words, the nature of the excited states of these dyes is favorable for DSCs. For **8e**, the second strongly dipole-allowed excited-state that

Table 4 Computed wavelengths (oscillator strength between brackets), CT distance (Å), CT charge (e) and dipole moments (D) of the ground and excited states of the five dyes

Dye	$\lambda_{max}^{abs}(1)$/nm (f in a.u.)	d^{CT}/Å	q^{CT}/e	μ^{GS}/D	μ^{ES}/D
8a	407 (2.6)	5.2	0.6	7.4	22.6
8b	442 (2.1)	4.7	0.6	8.7	22.5
8c	452 (2.1)	4.4	0.6	9.6	22.5
8d	494 (2.0)	4.7	0.6	12.2	25.8
8e	516 (2.3)	5.1	0.6	10.2	25.2

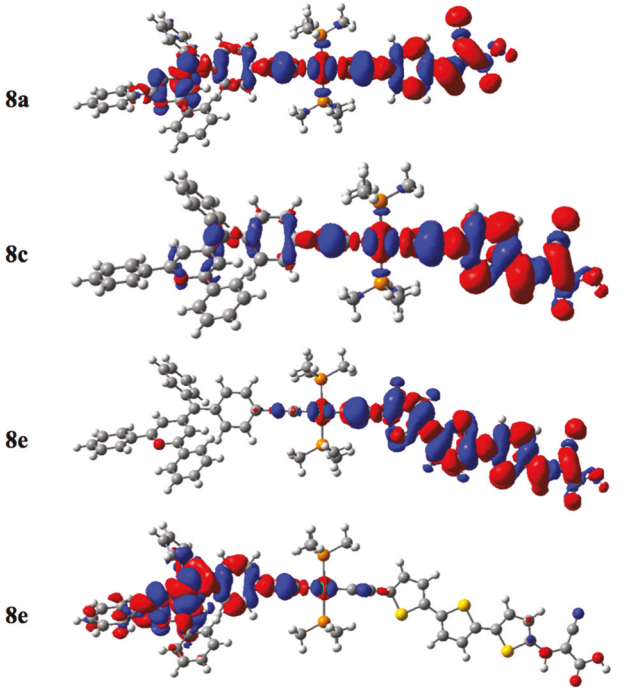

Fig. 6 Density difference plots for **8a**, **8c** and **8e**. For **8e** two plots corresponding to the first (top) and second (bottom) bands are displayed. The blue (red) regions indicate a decrease (increase) of the density upon photoabsorption.

corresponds to an experimental peak at *ca.* 390 nm is localized to the pyran side and the ethynyl segment. However, the computed CT distance in that case is trifling (1.09 Å), and it is unlikely that this band significantly contributes to energy conversion process. It can then be inferred that the CT character is therefore not the determining factor controlling the photovoltaic efficiency of these series of dyes. However, note that **8d** and **8e** present two specific features: absorption at a wavelength closer to the optimum for light harvesting and larger dipole moments (both at the ground and excited states), both characteristics being helpful to bend the conduction band of the semi-conductor and hence to inject charges.[40]

Photovoltaic properties in TiO_2 DSCs

The platinum complexes **8a–e** along with the reference benchmark sensitizer **N719** were tested in TiO_2 based solar cells with an iodide/triiodide based electrolyte (for composition see the Experimental part) and their performances were evaluated under AM 1.5 calibrated artificial sunlight. The photovoltaic characteristics (V_{oc}, J_{sc}, ff and PCE) of the solar cells are displayed in Table 5 and the photoaction spectra are shown in Fig. 7.

The photoconversion efficiencies (PCEs) steadily increase in the following order **8e** > **8d** > **8c** > **8b** > **8a** ranging from 1.70% (for **8a**) to 4.25% (for **8e**). Since the photopotentials and fill factors stay similar throughout the entire series, this constant rise in the PCE is essentially due to an improved short circuit current, increasing from 4.89 mA cm^{-2} (**8a**) to 12.54 mA cm^{-2}

Table 5 Photovoltaic performances for complexes **8a–e** in DSCs recorded under stimulated AM 1.5 irradiation (100 mW cm^{-2})

Dye	V_{oc} (mV)	J_{sc} (mA cm^{-2})	FF (%)	PCE (%)
8a[a]	505	4.89	68.7	1.70
8a[b]	553	4.46	74.2	1.83
8b[a]	504	6.45	72.8	2.36
8b[b]	578	6.38	72.4	2.67
8c[a]	496	6.89	72.2	2.47
8c[b]	563	6.84	72.3	2.78
8d[a]	513	10.0	68.5	3.52
8d[b]	562	10.15	70.9	4.04
8e[a]	496	12.54	68.3	4.25
8e[b]	554	12.01	70.4	4.69
N719[c]	721	15.23	69.4	7.60

[a] Without *tert*-butylpyridine in the electrolyte. [b] In the presence of 0.1 M *tert*-butylpyridine in the electrolyte. [c] In the presence of 0.5 M *tert*-butylpyridine in the electrolyte. For details see experimental details in ESI.

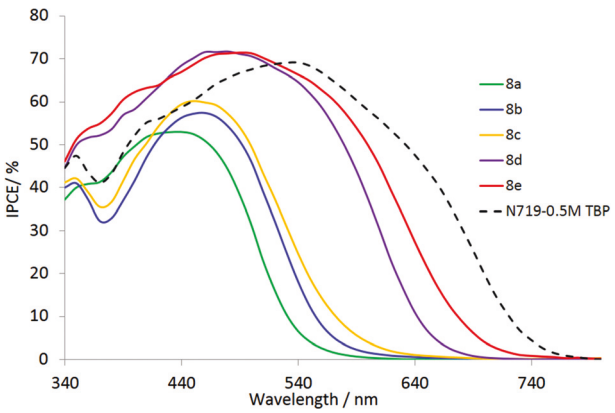

Fig. 7 Photoaction spectra (IPCE as a function of the incident wavelength) of the solar cells sensitized with dyes **8a–e** and **N719**.

(**8e**) (Table 4). As mentioned above, the reason for such differences cannot be assigned to thermodynamics (see Electrochemical measurements). However, UV-Vis absorption spectra show a steady red-shift of the main absorption peaks upon increasing the conjugation of the spacer, from **8a** to **8e**. This feature is observed both in solution and on TiO_2 transparent electrodes with onset absorptions ranging from 470 nm (**8a**) to 610 nm (**8e**). A red-shifted absorption of the photoelectrode is always considered a significant advantage since it allows for a better spectral matching with incident solar light and a concomitant increase of the photocurrent density. This logically translates into a constantly broadening LHE (light harvesting efficiencies) from **8a** to **8e**, and it is obviously illustrated by the IPCE, increasing from 53% at 440 nm to 71% at 500 nm, and spreading until 550 nm to 700 nm, for **8a** and **8e** respectively (Fig. 7). Interestingly, the incident photon to current efficiency (IPCE) of **8d** and **8e** is as high as that of the **N719** reference, meaning that the injection efficiency of the latter is quite optimized. On the other hand, as noted in the computational study, the second band of **8e** around 400 nm is not as effective as the first one around 510 nm to produce electricity. Indeed, the IPCE value around 400 nm is not as high as that around 510 nm probably because the charge shift of the excited-state is not optimal for electron injection (taking the place of the pyran moiety).

The values of the photopotentials were rather low (*ca.* 500 mV); in order to increase these values, *tert*-butylpyridine 0.1 M was added into the electrolyte.[41] An increase of 50–60 mV was recorded for all devices, with a very moderate loss in J_{sc}, implying an overall significant rise of the PCE (Table 5). The simultaneous effects of conduction band bending and surface defects passivation by *tert*-butylpyridine are likely responsible for this observation. Addition of greater amounts of *tert*-butylpyridine (0.5 M) led to an important decrease of the short circuit current (*ca.* 30%), likely because of a more sluggish electron injection process.

To sum up, the worst PCE was obtained for **8a** while the best was obtained for **8e**, featuring respectively the narrowest and broadest coverage of the visible spectrum among the whole series. Noticeably, V_{oc} values remained rather low for all complexes; the peak value reaches 578 mV for **8b;** by comparison benchmark **N719** exhibited more than 700 mV. This could explain a lower band bending induced by the permanent dipole moment of the chemisorbed dye, or – more likely – due to a faster charge recombination. Moreover, since the oxidation of iodide into triiodide is a multielectronic process, the use of the redox potential of the $E(I_2^-/I^-)$ couple over $E(I_3^-/I^-)$ is considered a better approximation to estimate the regeneration of the photo-oxidized dye.[42] In this case (Table 3), low regeneration driving forces were calculated and kinetics for this step could be slower than geminate charge recombination, thus entailing low values for the V_{oc}.

Conclusions and outlook

Five new platinum complexes (**8a–e**) were prepared and characterized in TiO_2 based DSCs. These five structures present a common pyran unit but differ by the linker separating the platinum from the cyanoacetic group. Voltammetry studies showed that, unlike their photoconversion efficiency, the oxidation potential of the compounds was not significantly changed by the nature or the size of the linker. In addition, exhaustive electrolysis indicated that the radical pyrilium cations for **8a–e** were relatively stable due to steric and electronic effects. Compound **8e**, which contains a trithiophene segment, gives a PCE of 4.7% in a dye-sensitized solar cell.

The theoretical calculations provided us with simulations of the experimental data and with insights into the nature of the excited states of the dyes, and showed that all five compounds present large but similar CT characteristics. In other words, the differences in the experimentally obtained PCE were not related to different CT efficiencies, but rather to differences in dipole moments and LHE.

The photovoltaic performances of the dye **8e** are relatively high for such platinum complexes and they are essentially limited by the LHE. Experiments are currently underway to

modify the structure of **8e** in order to enhance the LHE by red-shifting the maximum absorbance wavelength and consequently improving the photovoltaic performances.

Acknowledgements

We thank the US National Science Foundation (CHE-1153085), the European Research Council (ERC) and the *Région des Pays de la Loire* (Marches – 278845) for support. This research used resources of (1) the GENCI-CINES/IDRIS (c2014085117); (2) CCIPL (*Centre de Calcul Intensif des Pays de Loire*); and (3) the Troy cluster.

Notes and references

1 A. Hagfeldt, G. Boschloo, L. Sun, L. Kloo and H. Pettersson, *Chem. Rev.*, 2010, **110**, 6595–6663.

2 (*a*) A. S. Polo, M. K. Itokazu and N. Y. Murakami Iha, *Coord. Chem. Rev.*, 2004, **248**, 1343–1361; (*b*) J. N. Clifford, M. Planells and E. Palomares, *J. Mater. Chem.*, 2012, **22**, 24195–24201; (*c*) K. C. D. Robson, P. G. Bomben and C. P. Berlinguette, *Dalton Trans.*, 2012, **41**, 7814–7829; (*d*) G. C. Vougioukalakis, A. I. Philippopoulos, T. Stergiopoulos and P. Falaras, *Coord. Chem. Rev.*, 2011, **255**, 2602–2621.

3 (*a*) S. Archer and J. A. Weinstein, *Coord. Chem. Rev.*, 2012, **256**, 2530–2561; (*b*) F.-R. Dai, Y.-C. Chen, L.-F. Lai, W.-J. Wu, C.-H. Cui, G.-P. Tan, X.-Z. Wang, J.-T. Lin, H. Tian and W.-Y. Wong, *Chem. – Asian J.*, 2012, **7**, 1426–1434; (*c*) E. A. M. Geary, N. Hirata, J. Clifford, J. R. Durrant, S. Parsons, A. Dawson, L. J. Yellowlees and N. Robertson, *Dalton Trans.*, 2003, 3757–3762; (*d*) E. A. M. Geary, L. J. Yellowlees, L. A. Jack, I. D. H. Oswald, S. Parsons, N. Hirata, J. R. Durrant and N. Robertson, *Inorg. Chem.*, 2005, **44**, 242–250; (*e*) A. Islam, H. Sugihara, K. Hara, L. P. Singh, R. Katoh, M. Yanagida, Y. Takahashi, S. Murata, H. Arakawa and G. Fujihashi, *Inorg. Chem.*, 2001, **40**, 5371–5380; (*f*) E. C.-H. Kwok, M.-Y. Chan, K. M.-C. Wong, W. H. Lam and V. W.-W. Yam, *Chem. – Eur. J.*, 2010, **16**, 12244–12254; (*g*) L. P. Moorcraft, A. Morandeira, J. R. Durrant, J. R. Jennings, L. M. Peter, S. Parsons, A. Turner, L. J. Yellowlees and N. Robertson, *Dalton Trans.*, 2008, 6940–6947; (*h*) W. Wu, X. Xu, H. Yang, J. Hua, X. Zhang, L. Zhang, Y. Long and H. Tian, *J. Mater. Chem.*, 2011, **21**, 10666–10671; (*i*) W. Wu, J. Zhang, H. Yang, B. Jin, Y. Hu, J. Hua, C. Jing, Y. Long and H. Tian, *J. Mater. Chem.*, 2012, **22**, 5382–5389.

4 (*a*) M. Hissler, J. E. McGarrah, W. B. Connick, D. K. Geiger, S. D. Cummings and R. Eisenberg, *Coord. Chem. Rev.*, 2000, **208**, 115–137; (*b*) J. A. G. Williams, *Top. Curr. Chem.*, 2007, **281**, 205–268.

5 (*a*) S. Leininger, P. J. Stang and S. Huang, *Organometallics*, 1998, **17**, 3981–3987; (*b*) R. Chakrabarty, P. S. Mukherjee and P. J. Stang, *Chem. Rev.*, 2011, **111**, 6810–6918; (*c*) K. Ghosh, J. Hu, H. S. White and P. J. Stang, *J. Am. Chem. Soc.*, 2009, **131**, 6695–6697; (*d*) K. Ghosh, H.-B. Yang, B. H. Northrop, M. M. Lyndon, Y.-R. Zheng, D. C. Muddiman and P. J. Stang, *J. Am. Chem. Soc.*, 2008, **130**, 5320–5334; (*e*) X.-D. Xu, H.-B. Yang, Y.-R. Zheng, K. Ghosh, M. M. Lyndon, D. C. Muddiman and P. J. Stang, *J. Org. Chem.*, 2010, **75**, 7373–7380; (*f*) G.-Z. Zhao, Q.-J. Li, L.-J. Chen, H. Tan, C.-H. Wang, D.-X. Wang and H.-B. Yang, *Organometallics*, 2011, **30**, 5141–5146.

6 W.-Y. Wong and P. D. Harvey, *Macromol. Rapid Commun.*, 2010, **31**, 671–713.

7 (*a*) A. Y.-Y. Tam, K. M.-C. Wong and V. W.-W. Yam, *J. Am. Chem. Soc.*, 2009, **131**, 6253–6260; (*b*) F. Paul and C. Lapinte, *Coord. Chem. Rev.*, 1998, **178–180**(Part 1), 431–509; (*c*) R. Ziessel, M. Hissler, A. El-ghayoury and A. Harriman, *Coord. Chem. Rev.*, 1998, **178–180**(Part 2), 1251–1298; (*d*) A. Scarpaci, C. Monnereau, N. Hergue, E. Blart, S. Legoupy, F. Odobel, A. Gorfo, J. Perez-Moreno, K. Clays and I. Asselberghs, *Dalton Trans.*, 2009, 4538–4546.

8 (*a*) S. Suzuki, Y. Matsumoto, M. Tsubamoto, R. Sugimura, M. Kozaki, K. Kimoto, M. Iwamura, K. Nozaki, N. Senju, C. Uragami, H. Hashimoto, Y. Muramatsu, A. Konno and K. Okada, *Phys. Chem. Chem. Phys.*, 2013, **15**, 8088–8094; (*b*) C. C. Chang, B. Pfennig and A. B. Bocarsly, *Coord. Chem. Rev.*, 2000, **208**, 33–45; (*c*) P. Du, J. Schneider, P. Jarosz, J. Zhang, W. W. Brennessel and R. Eisenberg, *J. Phys. Chem. B*, 2007, **111**, 6887–6894; (*d*) J. E. McGarrah, Y.-J. Kim, M. Hissler and R. Eisenberg, *Inorg. Chem.*, 2001, **40**, 4510–4511; (*e*) T. J. Wadas, S. Chakraborty, R. J. Lachicotte, Q.-M. Wang and R. Eisenberg, *Inorg. Chem.*, 2005, **44**, 2628–2638; (*f*) P. Du, K. Knowles and R. Eisenberg, *J. Am. Chem. Soc.*, 2008, **130**, 12576–12577; (*g*) P. Jarosz, P. Du, J. Schneider, S.-H. Lee, D. McCamant and R. Eisenberg, *Inorg. Chem.*, 2009, **48**, 9653–9663.

9 R. Andreu, L. Carrasquer, S. Franco, J. Garín, J. Orduna, N. Martínez de Baroja, R. Alicante, B. Villacampa and M. Allain, *J. Org. Chem.*, 2009, **74**, 6647–6657.

10 (*a*) N. Faux, B. Caro, F. Robin-Le Guen, P. Le Poul, K. Nakatani and E. Ishow, *J. Organomet. Chem.*, 2005, **690**, 4982–4988; (*b*) E. Galan, R. Andreu, J. Garin, J. Orduna, B. Villacampa and B. E. Diosdado, *Org. Biomol. Chem.*, 2012, **10**, 8684–8691; (*c*) A. B. Marco, R. Andreu, S. Franco, J. Garín, J. Orduna, B. Villacampa and R. Alicante, *Tetrahedron*, 2013, **69**, 3919–3926.

11 S. Franco, J. Garín, N. Martínez de Baroja, R. Pérez-Tejada, J. Orduna, Y. Yu and M. Lira-Cantú, *Org. Lett.*, 2012, **14**, 752–755.

12 (*a*) F. Labat, T. Le Bahers, I. Ciofini and C. Adamo, *Acc. Chem. Res.*, 2012, **45**, 1268–1277; (*b*) B. Schulze, D. Escudero, C. Friebe, R. Siebert, H. Görls, S. Sinn, M. Thomas, S. Mai, J. Popp, B. Dietzek, L. González and U. S. Schubert, *Chem. – Eur. J.*, 2012, **18**, 4010–4025; (*c*) F. Nunzi, E. Mosconi, L. Storchi, E. Ronca, A. Selloni, M. Gratzel and F. De Angelis, *Energy Environ. Sci.*, 2013, **6**, 1221–1229.

13 (*a*) T. Le Bahers, C. Adamo and I. Ciofini, *J. Chem. Theory Comput.*, 2011, **7**, 2498–2506; (*b*) I. Ciofini, T. Le Bahers, C. Adamo, F. Odobel and D. Jacquemin, *J. Phys. Chem. C*, 2012, **116**, 11946–11955; (*c*) D. Jacquemin, T. L. Bahers, C. Adamo and I. Ciofini, *Phys. Chem. Chem. Phys.*, 2012, **14**, 5383–5388.

14 E. Matern, J. Pikies and G. Z. Fritz, *Anorg. Allg. Chem.*, 2000, **626**, 2136.

15 (*a*) A. Bolag, M. Mamada, J.-i. Nishida and Y. Yamashita, *Chem. Mater.*, 2009, **21**, 4350–4352; (*b*) A. Bolag, J. Nishida, K. Hara and Y. Yamashita, *Chem. Lett.*, 2011, **40**, 510–511.

16 J.-L. Fillaut, J. Perruchon, P. Blanchard, J. Roncali, S. Golhen, M. Allain, A. Migalsaka-Zalas, I. V. Kityk and B. Sahraoui, *Organometallics*, 2005, **24**, 687–695.

17 *Frambo 4.1.05, Program for Data Collection on Area Detectors*, BRUKER-Nonius Inc., 5465 East Cheryl Parkway, Madison, WI 53711-5373 USA.

18 G. M. Sheldrick, *Cell_Now (version 2008/1): Program for Obtaining Unit Cell Constants from Single Crystal Data*, University of Göttingen, Germany.

19 APEX2, *Program for Data Collection and Integration on Area Detectors*, BRUKER AXS Inc., 5465 East Cheryl Parkway, Madison, WI 53711-5373 USA.

20 G. M. Sheldrick, *Acta Crystallogr., Sect. A: Fundam. Crystallogr.*, 2008, **64**, 112–122.

21 O. V. Dolomanov, L. J. Bourhis, R. J. Gildea, J. A. K. Howard and H. Puschmann, *J. Appl. Crystallogr.*, 2009, **42**, 339–341.

22 (*a*) A. L. Spek, *PLATON, a multipurpose crystallographic tool*, Utrecht University, Utrecht, The Netherlands, 2008; (*b*) A. L. Spek, *J. Appl. Crystallogr.*, 2003, **36**, 7–13.

23 M. J. Frisch, *et al.*, *GAUSSIAN 09 (Revision D.01)*, Gaussian Inc., Wallungford CT, 2009.

24 C. Adamo and V. Barone, *J. Chem. Phys.*, 1999, **110**, 6158–6170.

25 T. Yanai, D. P. Tew and N. C. Handy, *Chem. Phys. Lett.*, 2004, **393**, 51–57.

26 J. Tomasi, B. Mennucci and R. Cammi, *Chem. Rev.*, 2005, **105**, 2999–3094.

27 The added polarization functions are an f orbital with α = 0.993 for Pt and a d orbital with α of 0.587, 0.736, 0.961, 0.364 and 0.496 for C, N, O, P and S atoms, respectively.

28 The added diffuse functions are s, p and d orbitals of the respective exponents of 0.0167, 0.0122 and 0.0301 for Pt. For the second and third row atoms, an sp function was added, with α of 0.0438, 0.0639, 0.0845, 0.0348 and 0.0405 for C, N, O, P and S atoms, respectively.

29 S. Rigaut, J. Perruchon, S. Guesmi, C. Fave, D. Touchard and P. H. Dixneuf, *Eur. J. Inorg. Chem.*, 2005, **2005**, 437–437.

30 A. Bolag, J.-i. Nishida, K. Hara and Y. Yamashita, *Org. Electron.*, 2012, **13**, 425–431.

31 K. Onitsuka, N. Ohara, F. Takei and S. Takahashi, *Dalton Trans.*, 2006, 3693–3698.

32 W. Wu, J. Zhao, J. Sun, L. Huang and X. Yi, *J. Mater. Chem. C*, 2013, **1**, 705–716.

33 (*a*) S. B. Gauthier, N. Weisbach, N. Bhuvanesh and J. A. Gladysz, *Organometallics*, 2009, **28**, 5597–5599; (*b*) M.-H. Nguyen and J. H. K. Yip, *Organometallics*, 2012, **31**, 7522–7531.

34 (*a*) T. B. Peters, J. C. Bohling, A. M. Arif and J. A. Gladysz, *Organometallics*, 1999, **18**, 3261–3263; (*b*) W. Mohr, J. Stahl, F. Hampel and J. A. Gladysz, *Chem. – Eur. J.*, 2003, **9**, 3324–3340.

35 N. Hirata, J.-J. Lagref, E. J. Palomares, J. R. Durrant, M. K. Nazeeruddin, M. Gratzel and D. Di Censo, *Chem. – Eur. J.*, 2004, **10**, 595–602.

36 The redox potential of the Fc^+/Fc couple in CH_2Cl_2/NBu_4PF_6 was measured experimentally with reference to the standard calomel electrode (SCE): $E^0(Fc^+/Fc)$ = 0.47 V *vs.* SCE. Recalibration *vs.* NHE was made considering that E^0(SCE) = 0.24 V *vs.* NHE. See ref: A. Bard and L. Faulkner, *Electrochemical methods*, J. Wiley & Sons, 2nd edn, 2001, p. 809.

37 S. Gauthier, N. Vologdin, S. Achelle, A. Barsella, B. Caro and F. Robin-le Guen, *Tetrahedron*, 2013, **69**, 8392–8399.

38 (*a*) F. Ba, N. Cabon, P. Le Poul, S. Kahlal, J.-Y. Saillard, N. Le Poul, S. Golhen, B. Caro and F. Robin-Le Guen, *New J. Chem.*, 2013, **37**, 2066–2081; (*b*) F. Ba, F. Robin-Le Guen, N. Cabon, P. Le Poul, S. Golhen, N. Le Poul and B. Caro, *J. Organomet. Chem.*, 2009, **695**, 235–243.

39 A. D. Laurent and D. Jacquemin, *Int. J. Quantum Chem.*, 2013, **113**, 2019–2039.

40 (*a*) U. B. Cappel, S. M. Feldt, J. Schöneboom, A. Hagfeldt and G. Boschloo, *J. Am. Chem. Soc.*, 2010, **132**, 9096–9101; (*b*) S. Rühle, M. Greenshtein, S. G. Chen, A. Merson, H. Pizem, C. S. Sukenik, D. Cahen and A. Zaban, *J. Phys. Chem. B*, 2005, **109**, 18907–18913.

41 G. Boschloo, L. Häggman and A. Hagfeldt, *J. Phys. Chem. B*, 2006, **110**, 13144–13150.

42 (*a*) R. Jono, M. Sumita, Y. Tateyama and K. Yamashita, *J. Phys. Chem. Lett.*, 2012, **3**, 3581–3584; (*b*) G. Boschloo and A. Hagfeldt, *Acc. Chem. Res.*, 2009, **42**, 1819–1826.